Published in
Journal of Materials Science : Materials in Electronics 19, issues 8-9, 821-827, 2008
which should be used for any reference to this work

Latest developments in GaN-based quantum devices for infrared optoelectronics

Eva Monroy · Fabien Guillot · Sylvain Leconte · Laurent Nevou · Laetitia Doyennette · Maria Tchernycheva · Francois H. Julien · Esther Baumann · Fabrizio R. Giorgetta · Daniel Hofstetter

Abstract In this work, we summarize the latest progress in intersubband devices based on GaN/AlN nanostructures for operation in the near-infrared. We first discuss the growth and characterization of ultra-thin GaN/AlN quantum well and quantum dot superlattices by plasma-assisted molecular-beam epitaxy. Then, we present the performance of nitride-based infrared photodetectors and electro-optical modulators operating at 1.55 μm. Finally, we discuss the progress towards intersubband light emitters, including the first experimental observation of intersubband photoluminescence in nitride nanostructures.

1 Introduction

Intersubband (ISB) transitions in semiconductor quantum wells (QWs) have found several device applications in the mid- and far- infrared spectral regions, such as quantum well infrared photodetectors and quantum cascade lasers [9, 27]. In the last years, research efforts have focused on extending the spectral region covered by ISB devices towards the near-infrared. Material systems with large enough conduction band offsets to accommodate ISB transitions at relatively short wavelengths (1.3, 1.55 μm) include InGaAs/AlAsSb [14] (CdS/ZnSe)/BeTe [2], and GaN/AlGaN QWs [11, 12, 17, 26, 32, 36, 37]. A specific advantage of III-nitrides is their extremely short ISB absorption recovery times ($\sim$150–400 fs [16, 22, 23]) due to the strong electron-phonon interaction in these materials, which open the way to devices operating in the 0.1–1 Tbit/s bit-rate regime. Furthermore, the wide bandgap of nitride semiconductors prevents two-photon absorption in the near-infrared, and devices would profit from other advantages of nitride technology, such as high power handling and chemical and thermal robustness.

In spite of these promising properties, the development of nitride-based ISB devices is in a very early stage. The first photovoltaic quantum well infrared photodetector was reported in 2003 [19], and the first photoconductor device has been recently reported [3]. All-optical switches operating at 1.5 μm have also been recently presented [24]. In this work, we summarize the latest progress in electro-optical ISB devices based on GaN/AlN nanostructures for operation in the near-infrared. We first discuss the growth and characterization of GaN/AlN quantum well and quantum dot superlattices (SLs) by plasma-assisted molecular-beam epitaxy. Then, we describe the performance of nitride-based ISB photodetectors and electro-optical modulators operating at 1.55 μm. Finally, we discuss the progress towards ISB light emitters.

2 Material growth

Due to the rather large electron effective mass of GaN ($m^* = 0.2m_0$), layers as thin as 1–1.5 nm are required to

E. Monroy (✉) · F. Guillot · S. Leconte
Equipe mixte CEA-CNRS Nanophysique et Semiconducteurs, DRFMC/SP2M/PSC, CEA-Grenoble, 17 rue des Martyrs, 38054 Grenoble cedex 9, France
e-mail: eva.monroy@cea.fr

L. Nevou · L. Doyennette · M. Tchernycheva · F. H. Julien
Action OptoGaN, Institut d'Electronique Fondamentale, Université Paris-Sud, UMR 8622 CNRS, 91405 Orsay cedex, France

E. Baumann · F. R. Giorgetta · D. Hofstetter
University of Neuchâtel, 2000 Neuchatel, Switzerland

achieve ISB absorptions at 1.3–1.55 μm. Plasma-assisted molecular-beam epitaxy (PAMBE) is the most suitable growth technique for this application, due to the low growth temperature, which hinders GaN-AlN interdiffusion and provides atomically abrupt interfaces [34]. Furthermore, in situ monitoring of the surface morphology by reflection high energy electron diffraction (RHEED) makes possible to control the growth at the atomic layer scale.

2.1 Quantum well structures

Al(Ga)N/GaN multiple-quantum-well (MQW) structures have been synthesized by PAMBE on 1-μm-thick AlN-on-sapphire templates. The growth rate was fixed at $\sim$0.3 monolayers per second (ML/s) by the flux of active nitrogen. Best GaN structural quality is achieved by depostion under Ga-rich conditions with 2 monolayers (ML) of Ga-excess segregating at the growth front [1]. In the case of AlN, the Al flux is fixed to the Al/N stoichiometric value and an additional Ga flux is introduced to stabilize the surface. Since the Al-N binding energy is much higher than the Ga-N binding energy, Ga segregates on the surface and it is not incorporated into the AlN layer.

The quality of the GaN/AlN heterostructures was found to be particularly sensitive to the Ga/N ratio. The strain fluctuations induced by Si doping and by the presence of the AlN barriers favor the formation of V-shaped pits, even in layers grown in the regime of 2 ML Ga-excess [18, 28]. The suppression of these defects has been achieved by an enhancement of the Ga-flux so that growth is performed at the limit of Ga-accumulation.

Regarding the growth temperature, it has been observed that overgrowth of GaN quantum wells with AlN at high temperatures results in an irregular thinning of the quantum well thickness due to exchange of Ga-atoms in the GaN layer with Al [13]. This is a thermally activated phenomenon that becomes relevant for AlN growth temperatures above 730 °C.

In conclusion, best interface results were achieved at a substrate temperature T_S = 720 °C, growing AlN at the Al/N stoichiometry without growth interruptions and using also Ga as a surfactant during the growth of AlN barriers. Under these conditions, the samples present a flat surface morphology with an rms surface roughness of 1.0–1.5 nm measured in an area of 5 × 5 μm^2. High-resolution transmission electron microscopy (HRTEM) shows homogeneous QWs, with an interface roughness of $\sim$1 ML (see interface analysis in ref. [34]). Figure 1 shows the ω–2θ scan of the (0002) X-ray refection of Si-doped GaN/AlN SLs with 1.5 nm QWs and variable barrier width. The presence of high-order peaks confirms an excellent structure periodicity.

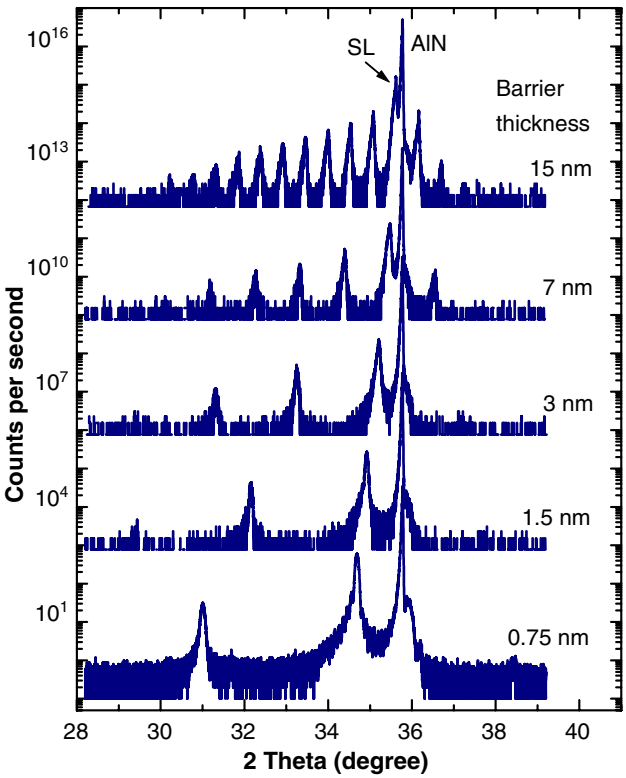

Fig. 1 ω–2θ scan of the (0002) X-ray refection of Si-doped GaN/AlN superlattices with 1.5 nm QWs and variable barrier width

2.2 Quantum dot structures

GaN/AlN quantum dot (QD) SLs have been synthesized by PAMBE on 1-μm-thick AlN-on-sapphire templates. The growth of self-assembled QDs is achieved by deposition of GaN on an AlN surface under N-rich conditions, at a Ga-limited growth rate of 0.25 ML/s. Under these conditions, growth starts two-dimensional until the deposition of a 2-ML-thick wetting layer. Due to the lattice mismatch between AlN and GaN, further GaN deposition leads to the formation of three-dimensional islands (Stranski-Krastanov growth mode) [7, 15]. The QD formation was monitored by RHEED, which showed rapid increase of the *a*-axis lattice parameter and of the RHEED intensity, with appearance of a spotty RHEED pattern. The synthesis of each GaN QD plane is followed by a growth interruption under vacuum, during which additional reflections corresponding to the QD facets become visible in the RHEED pattern. These GaN QDs are hexagonal truncated pyramids with {1–103} facets [6], and no Ga-Al interdiffusion has been observed [33]. The QDs were *n*-type doped by incorporating a silicon flux during the GaN deposition. We have demonstrated that Si doping does not modify the QD growth kinetics or morphology [15].

The QD size can be tuned by modifying the amount of GaN in the QDs, the growth temperature, or the growth

interruption time (Ostwald ripening). By adjusting the growth conditions, QDs with height (diameter) within the range of 1–1.5 nm (10–40 nm), and density between 10^{11} and 10^{12} cm^{-2} can be synthesized, as illustrated in the AFM image (Fig. 2). To populate the first electronic level, silicon can be incorporated into the QDs without significant perturbation of the QD morphology.

3 Quantum well infrared photodetectors

For the design of quantum well infrared photodetectors, the ISB absorption of a series of 20-period Si-doped AlN/GaN MQW structures with 2–3 nm AlN barriers and various GaN QW thicknesses was investigated using Fourier Transform infrared spectroscopy [37]. The sample facets were polished at 45° angle to form a multipass waveguide with 4–6 total internal reflections. The transmission for *p*- and *s*-polarized light was measured at room temperature using a deuterated triglycine sulfate photodetector. As an example, Fig. 3 shows the ISB absorption of Si-doped AlN/GaN MQWs with QW thickness of 4, 5, and 6 ML. The samples show a pronounced *p*-polarized absorption, attributed to transition from the first to the second electronic levels in the QW ($e_1 \rightarrow e_2$), while no absorption was found for *s*-polarized light within experimental accuracy. The spectra present Lorentzian shape, indicative of homogeneous broadening of the absorption. The line width of the absorption remains in the 70–120 meV range for QWs doped at 5×10^{19} cm^{-2}, and the ISB absorption efficiency per reflection attains 3–5%. A record bandwidth of $\sim$40 meV has been achieved in non-intentionally doped structures. The ISB absorption peak can be tuned in the 1.33–1.91 μm wavelength range by changing the QW thickness from 4 to 10 ML. For larger QWs, the $e_1 \rightarrow e_3$ transition is observed [37].

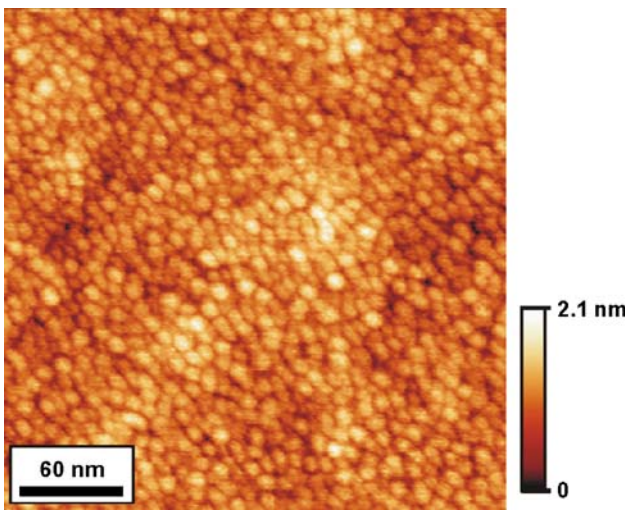

Fig. 2 Atomic force microscopy image of a sample with 20-periods of Si-doped GaN QDs with 3-nm-thick AlN barriers

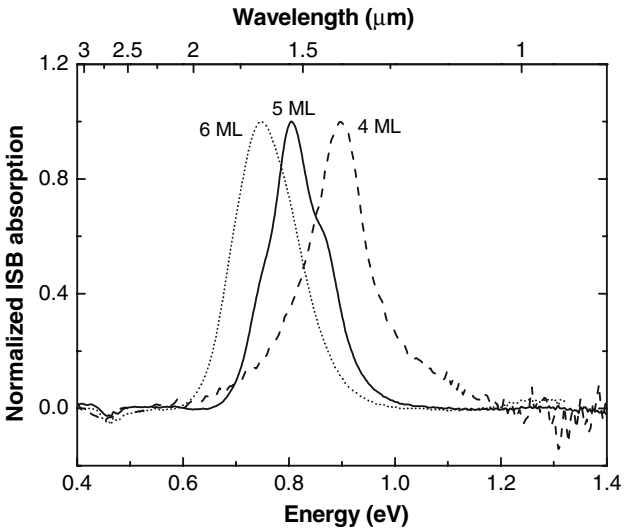

Fig. 3 Normalized *p*-polarized ISB absorption spectra of GaN/AlN superlattices with 3-nm-thick AlN barriers and different GaN QW thickness

In order to properly interpret the results and to apply them to device simulation, it is necessary to take into account the intense polarization fields in III-nitride materials. Indeed, it is well known that the optical properties of nitride QWs are strongly affected by the presence of an internal electric field [5]. This field, inherent to the wurtzite-phase nitride heterostructures grown along the [0001] axis, arises from the piezoelectric and spontaneous polarization discontinuity between the well and barrier materials. The polarization discontinuity is in the order of $\Delta P/\varepsilon_r\varepsilon_0$ = 10 MV/cm [37], where ΔP is the polarization discontinuity in Cm^{-2} and ε_r and ε_0 are the dielectric constant and the vacuum permittivity. Modeling of quantum confinement in nitride QWs should therefore go beyond the flat-band approximation and account for the internal electric field in the QW and in the barriers. As an example, Fig. 4 presents the conduction band diagram of a GaN QW in a GaN/AlN superlattice. The QW shape becomes triangular due to the intense electric field. This strong asymmetry of the electronic potential enables the observation of the $e_1 \rightarrow e_3$ in nitride QWs. Detailed modeling of ISB absorption of these samples is presented in ref. [37].

Photodetector devices were fabricated on AlN-capped GaN/AlN MQW structures, by evaporation of two Ti/Au contacts on the sample surface. The samples are cut and polished to form 45° multipass waveguides. Optical response spectra are obtained by illumination of one of the contacts through a single 45° facet, while the other contact is kept in the dark. The resulting photovoltage is amplified

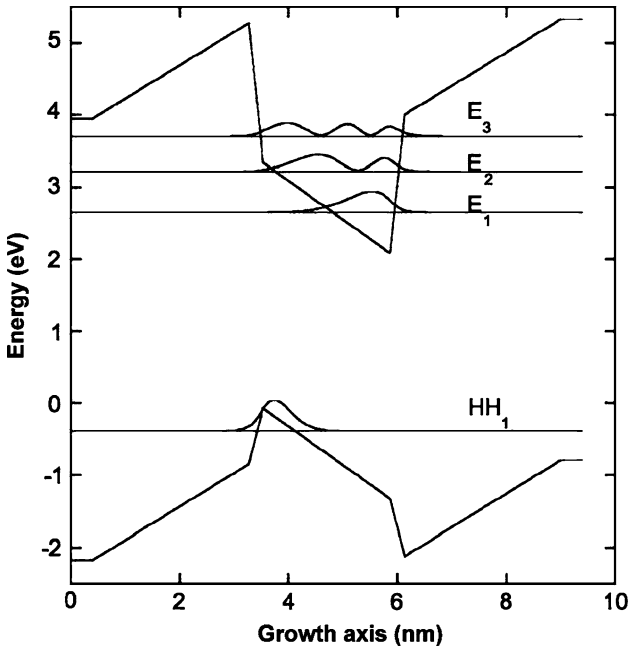

Fig. 4 Calculation of the energy levels in 2.6 nm thick GaN QWs in a superlattice with 3 nm AlN barriers. E_i indicates the electronic levels and HH indicate the first electronic level of the valence band

and fed into the external detector port of a Fourier transform infrared spectrometer.

Figure 5 presents the characterization of these devices as photovoltaic ISB photodetectors. In this experiment, the sample was illuminated by the white light source of the Fourier spectrometer. A photovoltage peak is observed around 1.5 μm, with a best FWHM of 90 meV. This extremely narrow peak confirms the good structural material quality. Typical responsivity values for samples with 40 GaN/AlN periods are about 8 μV/W [20].

We have tested the speed of such a detector at room temperature by exciting the device with a directly modulated diode laser beam at 1.55 μm. The voltage response is amplified by two consecutive voltage amplifiers (Sonoma 317 and Miteq AFS-5) and measured in a spectrum analyzer (Agilent E4407B). The highest frequency for which a signal is observed is 2.37 GHz [10]. Since the device package does not involve any optimization for high frequency testing, a substantial improvement is expected in future tests.

4 Quantum dot infrared photodetectors

Si-doped QD superlattices exhibit strong *p*-polarized intraband absorption at room-temperature, as shown in Fig. 6. The broadening of the absorption peak remains below 150 meV and can be as small as ∼80 meV for the most homogeneous samples. This absorption line is attributed to transition from the *s* ground level of the QD to the first excited level along the growth axis, p_z. The peak energies of both photoluminescence emission and intraband absorption are consistent with the QD structural characteristics and with their evolution by changing the growth conditions. Tuning of the intraband absorption from 0.740 (1.68 μm) to 0.896 eV (1.38 μm) is demonstrated.

Lateral QDIP devices have been fabricated in samples consisting of 20 periods of ∼1-nm-high Si-doped GaN QDs with 3-nm-thick AlN barriers deposited on AlN-on-sapphire templates. The sample facets have been mechanically polished at a 45° angle to form a multipass

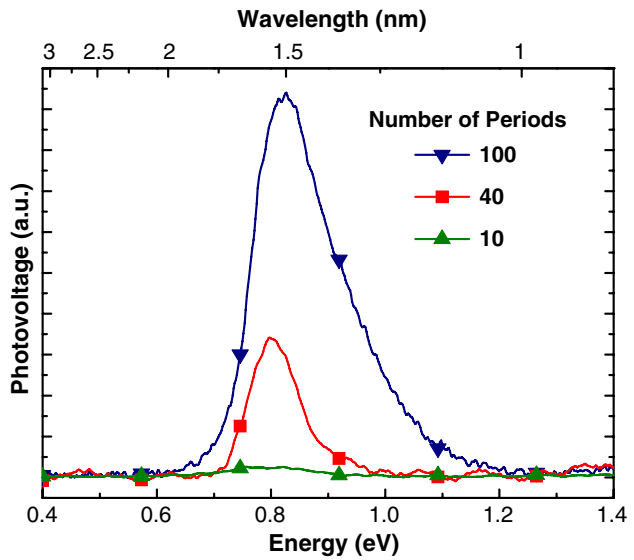

Fig. 5 Photovoltaic response of GaN/AlN QW infrared photodetectors with different number of periods

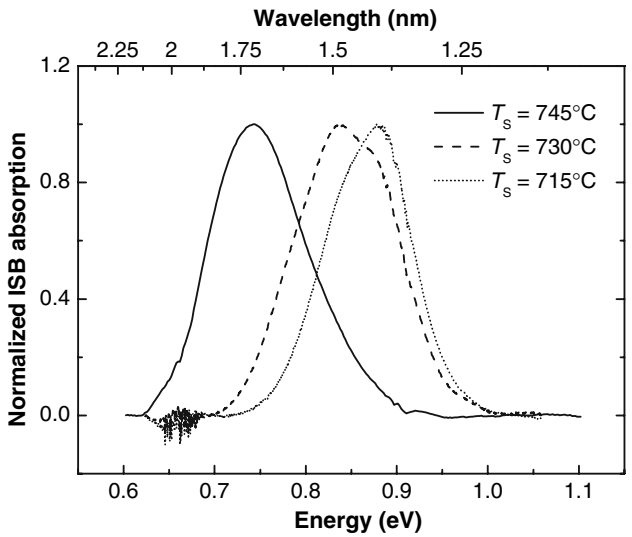

Fig. 6 Normalized *p*-polarized ISB absorption spectra of GaN/AlN QD superlattices grown at different substrate temperatures, T_S

waveguide with 5–6 total internal reflections for optical characterizations. Two Ti/Al/Ti/Au metal contacts were deposited on the surface, and annealed to enhance metal diffusion into the semiconductor layers.

The devices exhibit photocurrent only observed for TM-polarized light, following the intraband s–p_z selections rules. The fact that the photocurrent obeys the same selection rules and that its spectrum closely follows the intraband absorption are clear evidences that the photocurrent originates from the intraband transition of the nitride QDs. The photocurrent is explained by photoexcitation from the s electronic level to the p_z electronic level of the dots, followed by electrons transfer to the wetting layer ground state [8, 38]. This interpretation is further supported by the observation of an exponential increase of the photocurrent with temperature. The responsivity of these devices is about 8 mA/W at 300 K.

5 Electro-optical modulators

The first electro-absorption ISB modulation experiments on AlN/GaN SLs were based on the electrical depletion of a five period AlN/GaN (1.5/1.5 nm) SL grown on a thick GaN buffer. The absorption spectrum of such a sample presents two distinct peaks related to ISB transitions in the SL and in the two-dimensional electron gas located at the interface of the lowest SL barrier and the underlying GaN buffer. The ratio of those two absorption peaks can be adjusted by applying an external field (see Fig. 7), which influences the overall band structure and, more specifically, the free carrier density in the SL [4].

Room temperature intersubband electro-absorption modulation at telecommunication wavelengths has also been demonstrated in GaN/AlN coupled quantum wells with AlGaN contact layers [30]. The electro-modulation originates from electron tunneling between a wide well (reservoir) and a narrow well separated by an ultrathin (1 nm) AlN barrier. The maximum modulation depth with 0.8 V applied across the active region is $\sim$44% at 2.2 μm. The -3 dB cut-off frequency limited by the RC time constant is as high as 1.4 GHz for 10×10 μm^2 mesas, and could be further improved by reducing the access resistance of the AlGaN contact layers.

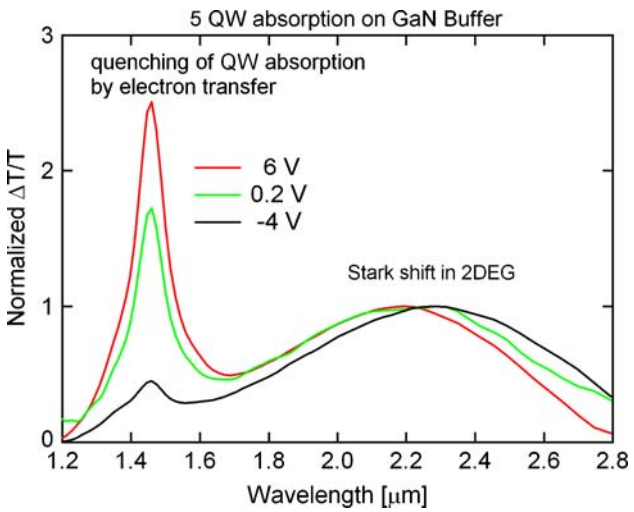

Fig. 7 Variation of the absorbance spectrum of a GaN/AlN ISB electro-optical modulator as a function of bias

6 Towards light emitters

ISB photoluminescence has been reported using GaN/AlN QWs designed to exhibit three bound states in the conduction band [29, 31]. Optical excitation in resonance with the e_1e_3 ISB transition is used to populate with electrons the e_3 subband. The emission arises from the radiative transition of electrons between the e_3 and e_2 subbands.

For room-temperature photoluminescence measurements, the input and output facets of the samples are polished at 45° angle and 90° angle, respectively. Excitation at $\lambda = 0.98$ μm in resonance with the e_1e_3 transition energy is provided by a tunable Ti : Sapphire laser operated in continuous wave under optical pumping by an Ar^{++} laser. The pump power is 1 W. The laser beam is focused at normal incidence onto the 45° input facet (power density 10^4 W cm^{-2}) and the pump beam experiences multipass reflections inside the sample. The emission beam is then directed to the emission port of the FTIR spectrometer, operated in step-scan mode. Detection is performed by a liquid nitrogen cooled InAs detector. The ISB PL spectra of a GaN/AlN SL is shown in Fig. 8 for p-polarized excitation. The emission is peaked at $\lambda = 2.13$ μm with a FWHM of 60 meV. The luminescence is mainly p-polarized, the ratio between p- and s-polarization exceeding a factor of 3. The residual s-polarized signal is probably due to depolarization effects because of multiple reflections inside the sample. These results prove the feasibility of optically pumped ISB emitting devices. However, in order to develop quantum fountain lasers, further work is required in terms of growth optimization, processing and dedicated laser active region and cavity design.

Regarding electrically injected ISB light emitters, a number of structure designs have been reported [21, 25, 35, 39]. However, to achieve efficient vertical current injection, it might be necessary to reduce drastically the dislocation density in these structures. This would imply the use of high-quality AlN substrates, currently under development, and an additional effort in strain engineering in the device design. Besides, further experiments aiming at a better understanding of resonant tunneling processes in

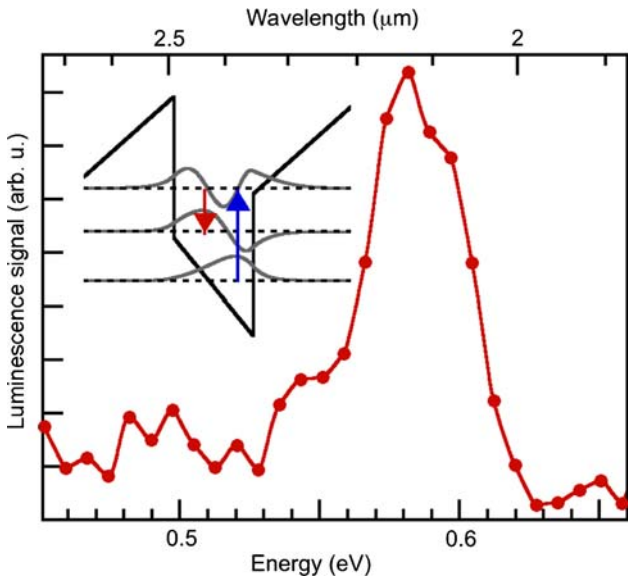

Fig. 8 Room-temperature intersubband luminescence spectrum under excitation at $\lambda = 0.98$ μm wavelength. The *inset* shows the conduction band profile and energy levels of an 8 ML thick QW

III-nitride heterostructures, and the role of threading dislocations in vertical electron transport must be carried out.

7 Conclusions

In conclusion, plasma-assisted molecular-beam epitaxy has proven its capability to synthesize short-period GaN/AlN QW and QD superlattices, compatible with intraband transitions at telecommunication wavelengths (1.3, 1.55 μm). First prototypes of photodetectors, electro-optical modulators and light emitters based on intraband transitions in III-nitride nanostructures have been demonstrated with promising performance.

Acknowledgments This work is supported by the 6th European Framework Program within NITWAVE project (STREP 004170). The AlN-on-sapphire templates used in this work were supplied by DOWA Electronics Materials Co., Ltd. Technical support from Y. Curé, Y. Genuist and M. Terrier is acknowledged.

References

1. C. Adelmann, J. Brault, G. Mula, B. Daudin, L. Lymperakis, J. Neugebauer, Phys. Rev. B **67**, 165419 (2003)
2. R. Akimoto, B.S. Li, K. Akita, T. Hasama, Appl. Phys. Lett. **87**, 181104 (2005)
3. E. Baumann, F.R. Giorgetta, D. Hofstetter, H. Lu, X. Chen, W.J. Schaff, L.F. Eastman, S. Golka, W. Schrenk, G. Strasser, Appl. Phys. Lett. **87**, 191102 (2005)
4. E. Baumann, F.R. Giorgetta, D. Hofstetter, S. Leconte, F. Guillot, E. Bellet-Amalric, E. Monroy, Appl. Phys. Lett. **89**, 101121 (2006)
5. F. Bernardini, V. Fiorentini, D. Vanderbilt, Appl. Phys. Lett. **56**, R10024 (1997)
6. V. Chamard, T. Schülli, M. Sztucki, T.H. Metzger, E. Sarigiannidou, J.-L. Rouvière, M. Tolan, C. Adelmann, B. Daudin, Phys. Rev. B **69**, 125327 (2004)
7. B. Daudin, F. Widmann, G. Feuillet, Y. Samson, M. Arlery, J.L. Rouvière, Phys. Rev. B **56**, R7069 (1997)
8. L. Doyennette, L. Nevou, M. Tchernycheva, A. Lupu, F. Guillot, E. Monroy, R. Colombelli, F.H. Julien, Electron. Lett. **41**, 1077–1078 (2005)
9. J. Faist, C. Sirtori, F. Capasso, L. Pfeiffer, K. West, Appl. Phys. Lett. **64**, 872 (1994)
10. F.R. Giorgetta, E. Baumann, F. Guillot, E. Monroy, D. Hofstetter, Electron. Lett. **43**, 185 (2007)
11. C. Gmachl, H.M. Ng, S.N.G. Chu, A.Y. Cho, Appl. Phys. Lett. **77**, 3722 (2000)
12. C. Gmachl, H.M. Ng, A.Y. Cho, Appl. Phys. Lett. **79**, 1590 (2001)
13. N. Gogneau, G. Jalabert, E. Monroy, E. Sarigiannidou, J.-L. Rouvière, T. Shibata, M. Tanaka, J.-M. Gérard, B. Daudin, J. Appl. Phys. **96**, 1104 (2004)
14. A.V. Gopal, H. Yoshida, A. Neogi, N. Georgiev, T. Mozume, T. Simoyama, O. Wada, H. Ishikawa, IEEE J. Quantum Electron. **38**, 1515 (2002)
15. F. Guillot, E. Bellet-Amalric, E. Monroy, M. Tchernycheva, L. Nevou, L. Doyennette, F.H. Julien, Le Si. Dang, T. Remmele, M. Albrecht, T. Shibata, M. Tanaka, J. Appl. Phys. **100**, 044326 (2006)
16. J.D. He, C. Gmachl, H.M. Ng, A.Y. Cho, Appl. Phys. Lett. **81**, 1803 (2002)
17. A. Helman, M. Tchernycheva, A. Lusson, E. Warde, F.H. Julien, Kh. Moumanis, G. Fishman, E. Monroy, B. Daudin, Le Si. Dang, E. Bellet-Amalric, D. Jalabert, Appl. Phys. Lett. **83**, 5196 (2003)
18. M. Hermann, E. Monroy, A. Helman, B. Baur, M. Albrecht, B. Daudin, O. Ambacher, M. Stutzmann, M. Eickhoff, Phys. Stat. Sol. (c) **1**, 2210 (2004)
19. D. Hofstetter, S.-S. Schad, H. Wu, W.J. Schaff, L.F. Eastman, Appl. Phys. Lett. **83**, 572 (2003)
20. D. Hofstetter, E. Baumann, F.R. Giorgetta, M. Graf, M. Maier, F. Guillot, E. Bellet-Amalric, E. Monroy, Appl. Phys. Lett. **88**, 121112 (2006)
21. D. Indjin, Z. Ikonic, V.D. Jovanovic, N. Vukmirovic, P. Harrison, R.W. Kelsall, Semicond. Sci. Technol. **20**, S237 (2005)
22. N. Iizuka, K. Kaneko, N. Suzuki, T. Asano, S. Noda, O. Wada, Appl. Phys. Lett. **77**, 648 (2000)
23. N. Iizuka, K. Kaneko, N. Suzuki, Appl. Phys. Lett. **81**, 1803 (2002)
24. N. Iizuka, K. Kaneko, N. Suzuki, IEEE J. Quantum Electron. **42**, 765 (2006)
25. A. Ishida, K. Matsue, Y. Inoue, H. Fujiyasu, H.J. Ko, A. Setiawan, J.J. Kim, H. Makino, T. Yao, Jpn. J. Appl. Phys. Part 2 **44**, 5918 (2005)
26. K. Kishino, A. Kikuchi, H. Kanazava, T. Tachibana, Appl. Phys. Lett. **81**, 1234 (2002)
27. B.F. Levine, J. Appl. Phys. **74**, R1 (1993)
28. T. Nakamura, S. Mochizuki, S. Terao, T. Sano, M. Iwaya, S. Kamiyama, H. Amano, I. Akasaki, J. Cryst. Growth. **237–239**, 1129 (2002)
29. L. Nevou, F.H. Julien, R. Colombelli, F. Guillot, E. Monroy, Electron. Lett. **42**, 1308 (2006)
30. L. Nevou, N. Kheirodin, M. Tchernycheva, L. Meignien, P. Crozat, A. Lupu, E. Warde, F.H. Julien, G. Pozzovivo, S. Golka, G. Strasser, F. Guillot, E. Monroy, T. Remmele, M. Albrecht, Appl. Phys. Lett. **90**, 223511 (2007)
31. L. Nevou, M. Tchernycheva, F.H. Julien, F. Guillot, E. Monroy, Appl. Phys. Lett. **90**, 121106 (2007)

32. S. Nicolay, J.F. Carlin, E. Feltin, R. Butte, M. Mosca, N. Grandjean, M. Ilegems, M. Tchernycheva, L. Nevou, F.H. Julien, Appl. Phys. Lett. **87**, 111106 (2005)
33. E. Sarigiannidou, E. Monroy, B. Daudin, J.L. Rouvière, A.D. Andreev, Appl. Phys. Lett. **87**, 203112 (2005)
34. E. Sarigiannidou, E. Monroy, N. Gogneau, G. Radtke, P. Bayle-Guillemaud, E. Bellet-Amalric, B. Daudin, J.L. Rouvière, Semicond. Sci. Technol. **21**, 912 (2006)
35. G. Sun, R.A. Soref, Microelectron. J **36**, 450 (2005)
36. N. Suzuki, N. Iizuka, Jpn. J. Appl. Phys. Suppl. **38**, L363 (1999)
37. M. Tchernycheva, L. Nevou, L. Doyennette, F.H. Julien, E. Warde, F. Guillot, E. Monroy, E. Bellet-Amalric, T. Remmele, M. Albrecht, Phys. Rev. B **73**, 125347 (2006)
38. A. Vardi, N. Akopian, G. Bahir, L. Doyennette, M. Tchernycheva, L. Nevou, F.H. Julien, F. Guillot, E. Monroy, Appl. Phys. Lett. **88**, 143101 (2006)
39. N. Vukmirovic, V.D. Jovanovic, D. Indjin, Z. Ikonic, P. Harrison, V. Milanovic, J. Appl. Phys. **97**, 103106 (2005)